On the identification of favourable factors for corrosion inhibition of aluminium by 8-hydroxyquinoline and its derivatives: DFT and electrochemical studies

Fatah Chiter, Yann Bulteau, Pierre Bonin, Nadine Pébère, Corinne Lacaze-Dufaure

Corrosion Science 233 (2024) 112104

Contents lists available at ScienceDirect

Corrosion Science

journal homepage: www.elsevier.com/locate/corsci

On the identification of favourable factors for corrosion inhibition of aluminium by 8-hydroxyquinoline and its derivatives: DFT and electrochemical studies

Fatah Chiter, Yann Bulteau, Pierre Bonin, Nadine Pébère *, Corinne Lacaze-Dufaure *

CIRIMAT, Toulouse INP, Université Toulouse 3 Paul Sabatier, CNRS, Université de Toulouse, 4 allée Emile Monso - BP44362, Toulouse 31030, France

ARTICLE INFO

Keywords:
A. Aluminium
B. Electrochemical measurements
B. Modelling studies
C. Interfaces
C. Neutral inhibition

ABSTRACT

Computational and electrochemical experimental approaches were combined to identify factors which would be favourable or detrimental to corrosion inhibition of aluminium by 8-hydroxyquinoline (*8Hq*) and its sulfonic derivative (*8HqSH*). *8HqSH* exhibited a strong adsorption on Al(111) but a greater solubility in water than *8Hq*, including Al complexes, which might increase Al corrosion. This was confirmed by the electrochemical measurements. In the presence of *8HqSH*, an acceleration of the aluminium dissolution was observed, whereas, in the presence of *8Hq*, a protective film was formed on the Al surface.

1. Introduction

The 8-hydroxyquinoline molecule (*8Hq*) has already been the purpose of numerous works due to a broad range of applications such as metal cations detection and removal [1–3], organic light emitting diodes (OLEDs) [4,5] and medicine [6]. Corrosion inhibition efficiency of *8Hq* has also been studied as it could be an environment-friendly candidate for the replacement of chromates for aluminium-based alloys [7–11]. All of these uses are based on the ability of the quinoline compound to complex metal ions. One of the most studied derivative of *8Hq* was the 8-hydroxyquinoline-5-sulfonic acid (*8HqSH*). As for the *8Hq* molecule, applications of such derivative is due to its chelating ability, in particular for metal ions detection in aqueous solutions [3,12]. Both molecules seem to have the same chemical reactivity towards complexation with metal ions. However, little is known on the *8HqSH* reactivity as potential corrosion inhibitor. It has even been classified as an aluminium corrosion accelerator [11,13].

In the field of corrosion inhibitors, correlations between electronic properties of the molecules and their inhibitive efficiency, experimentally determined, have been proposed and debated [14–17]. In parallel, the study of the inhibitor-metallic surface bonding has also been the purpose of several computational studies in relation with experimental identification of the inhibitive layer on the metal surface [8,10,18–20]. Other important factors are also relevant for corrosion inhibition. For instance, the molecules solubility in aqueous solution together with the possible formation of complexes with metal cations have to be taken into account. These two phenomena are competitive with the inhibitors adsorption on the metal surface and the formation of protective organic layers [21].

In our previous works, corrosion inhibition of pure aluminium by *8Hq* has been characterized by electrochemical and analytical techniques [7,9] and more recently, in addition to these experimental results, density functional theory (DFT) studies of the *8Hq*-aluminium and *8-Hq*-oxide covered aluminium surfaces bonding have been performed [22–26]. The present work aims first to investigate, at atomic scale, the action mechanisms of the *8Hq* and of the *8HqSH* on pure aluminium surfaces performing DFT calculations, including an implicit solvent model. Then, electrochemical measurements (polarisation curves and impedance spectroscopy) were performed on pure aluminium (99.9999 wt%) during immersion in a neutral aqueous solution in the presence of the two quinoline derivatives to evaluate their inhibitive action. Electrochemical techniques are the most used *in situ* techniques, at laboratory scale, to assess inhibition efficiency of organic compounds. Moreover, they are powerful to analyse the inhibitive action (anodic, cathodic or mixed) and to evaluate synergy effects [7,9,27]. Among the electrochemical techniques, impedance spectroscopy (EIS) presents several advantages, in particular to study adsorption kinetics of inhibitors or for *in situ* determination of thin organic layer thicknesses adsorbed onto metallic surfaces [28,29]. The final aim of the present study is to combine the modelling outputs with the electrochemical data

* Corresponding authors.
E-mail addresses: nadine.pebere@ensiacet.fr (N. Pébère), corinne.dufaure@ensiacet.fr (C. Lacaze-Dufaure).

https://doi.org/10.1016/j.corsci.2024.112104
Received 20 November 2023; Received in revised form 2 April 2024; Accepted 30 April 2024
Available online 4 May 2024

in order to extract the factors which are favourable to the inhibition processes or, in other words, to find descriptors correlated with the inhibitor efficiency. Hereafter, the computational details, with a description of models and equations of the energies calculated from the DFT computations, and the experimental procedure (materials and methods) are first specified. The results of the DFT studies are next presented and discussed: the solvation and solubility of the 8-hydroquinoline species (*8Hq* and *8HqSH*) were investigated in aqueous solution. The adsorption of the molecules on an Al(111) surface was then studied in terms of structures, energetics and charge distribution, in presence of an implicit solvent model. Following, the electrochemical results, *i.e.* open circuit variation, polarisation curves and electrochemical impedance diagrams without inhibitor, with *8Hq* or with *8HqSH*, allowed the inhibition effect of both quinoline molecules to be evaluated. The impedance data analysis, using the complex-capacitance representation (exploitation of the high-frequency part of the diagrams), make it possible to have a better understanding of the interface properties, as already pointed out in previous studies [28,30,31].

2. Computational details

The molecules studied are the 8-hydroxyquinoline (*8Hq*) and the 8-hydroxyquinoline-5-sulfonic acid (*8HqSH*). In the latter, a *H* atom of *8Hq* is substituted by a sulfonic group at the para position of the phenyl (Fig. 1).

DFT calculations were first carried out with the GAUSSIAN09 [32] package to study the solvation of the free molecules, their deprotonated species, and their complexes with Al^{3+} cations. Then, the VASP (Vienna Ab-initio Simulation Package) code [33–36] was used to investigate the molecules adsorption on the Al(111) surface in the framework of periodic calculations to give insight at the very first steps of the formation of organic layers on the aluminium surface.

2.1. Molecular calculations

The geometries of the native molecules and complexes (*molH*) and of the deprotonated species (mol^-) were first fully optimised in vacuum to investigate their Gibbs solvation energies and their solubilities. Spin polarised density functional theory calculations were performed with the GAUSSIAN09 package [32]. The PBE functional [37] with the def2TZVP basis set [38,39] and Grimme's D3 [40,41] dispersion corrections were chosen. All the stationary points were characterised as minima by a vibrational analysis. The total energy of the species included zero-point energy corrections and the calculated Gibbs energies at 298.15 K also included thermal corrections. In a second step, Gibbs energies were also calculated using Truhlar and coworkers' SMD solvation model [42] by placing the solute in a cavity within the solvent reaction field to model an aqueous solution.

Complexation Gibbs energies of the deprotonated species ($mol^- = q^-$, qSH^- and qS^{2-}) with an Al^{3+} cation were determined in water as:

$$\Delta G^{\circ}_{complexation} = G^{\circ}(complex) - \left(3 \quad G^{\circ}(mol^-) + \quad G^{\circ}\left(Al^{3+}\right)\right) \tag{1}$$

With $G^{\circ}(complex)$ the Gibbs energy of the complex of 3 molecules mol^- with Al^{3+}. The complexes studied are presented in Fig. 2.

To evaluate the affinity of all the species with water, the solvation Gibbs energies $\Delta G^{\circ}_{solvation}$ of the molecules were calculated. For the neutral species (*molH*), *i.e. 8Hq, 8HqSH, Alq₃* and *Al(qSH)₃*, the solvation Gibbs energies were calculated as:

$$\Delta G^{\circ}_{solvation}(molH) = \quad G^{\circ}_{in\ water}(molH) - \quad G^{\circ}_{in\ vacuum}(molH) \tag{2}$$

With $G^{\circ}_{in\ water}$ the total Gibbs energy of the molecule (*molH*) in water and $G^{\circ}_{in\ vacuum}$ the total Gibbs energy of the molecule (*molH*) in vacuum.

For the anionic species, q^-, qSH^- and qS^{2-}, and the $Al(qS)_3^{3-}$ complex, the solvation Gibbs energies were determined with the expression proposed by Truhlar *et al.* [43–45]:

$$\begin{aligned}\Delta G^{\circ}_{solvation}(mol^-) = \quad & -\Delta G^{\circ}_{g}(molH) + \quad \Delta G^{\circ}_{Solvation}(molH) \\ & + 2.303RT\ pKa(molH) - \quad \Delta G^{\circ}_{Solvation}(H^+) \\ & - \Delta G^{1atm \to 1mol}\end{aligned} \tag{3}$$

With $\Delta G^{\circ}_{Solvation}(molH)$ the solvation Gibbs energy of the neutral species *molH*, *pKa* the negative logarithm of its dissociation constant, and $\Delta G^{1atm \to 1mol} = 0.082$ eV (Gibbs energy change when moving from a gas-phase pressure of 1 atm to a liquid phase of concentration 1 M at 298.15 K).

$\Delta G^{\circ}_{g}(molH)$ is the gas-phase acidity of *molH* (see Table S1) calculated as:

$$\Delta G^{\circ}_{g}(molH) = G^{\circ}(mol^-) + \quad G^{\circ}(H^+) - G^{\circ}(molH) \tag{4}$$

With G° the Gibbs energy of the mol^-, H^+ and *molH* species in vacuum.

In the above expression a value of −11.53 eV was used for the absolute aqueous solvation free energy of the proton $\Delta G^{\circ}_{Solvation}(H^+)$ [45].

From the solvation Gibbs energies $\Delta G^{\circ}_{solvation}(molH)$, the solubility *S* of the native *8Hq* and *8HqSH* molecules was calculated [46]:

$$S(molH) = \frac{P^{\circ}_{molH}}{P^{\circ}} * \exp\left(\frac{-\Delta G^{\circ}_{solvation}(molH)}{RT}\right) \tag{5}$$

With P°_{molH} the pure substance vapour pressure of solid *(molH)* at 298 K, $P^{\circ} = 24.45$ atm (pressure of an ideal gas at 1 molar concentration and 298.15 K).

2.2. Periodic calculations

Periodic calculations with plane-wave basis set were chosen to study the adsorption of the molecules on an Al(111) surface, chosen to represent a bare aluminium surface. Indeed, at neutral pH, the thin protective aluminium oxide film can be defective and in this case, aggressive species in solution can be directly in contact with the bare metal surface.

The periodic calculations were performed using the VASP (Vienna Ab-initio Simulation Package) code [33–36] at the DFT-D level of

Species	X
8Hq	*H*
8HqSH	*SO₃H*
8HqS⁻	*SO₃⁻*

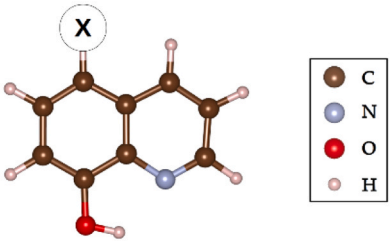

Fig. 1. *8Hq* species and derivatives.

Species	X
Alq₃	H
Al(qSH)₃	SO_3H
Al(qS)₃³⁻	SO_3^-

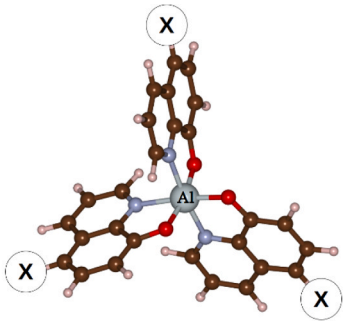

Fig. 2. Alq_3, $Al(qSH)_3$ and $Al(qS)_3^{3-}$ complexes.

theory. The PBE functional [37,47] and Grimme's D2 dispersion correction [40,41] were chosen. Potentials generated by the Projector augmented-wave method (PAW potentials) described the electrons/core interactions [48,49]. Calculations parameters included a cut-off energy of 450 eV for the plane-wave basis set, a Methfessel-Paxton smearing of the Fermi surface [50] with σ = 0.1 eV, an electronic convergence criterion of 10^{-6} eV and a convergence criterion on the forces on atoms smaller than 0.005 eV/Å for the geometry optimisations. The reciprocal space was sampled by a Monkhorst-Pack [51] grid of 3×3×1 k-points.

In this study, the coverage of the bare surface by molecules was θ = $4.72{\cdot}10^{-3}$ molecule/Å^2 (5×6 supercell). This low coverage allowed the very first steps of the organic layer formation on Al(111) to be simulated. The Al(111) surface was modelled by an asymmetric slab of four Al(111) layers, with the two top layers free to relax, and the two bottom layers fixed. The molecules were adsorbed on top of the Al(111) surface. The vacuum, measured from the top of the adsorbed molecule to the bottom of the adjacent slab was at least 14.4 Å.

Models of the deprotonated species of the *8Hq* and *8HqSH* molecules were adsorbed on the Al(111) surface. It has been shown previously that these species led to the strongest interaction with aluminium during the adsorption process in vacuum [22–26]. *q*, *qSH* and *qS* radicals, resulting from H-abstraction on the hydroxyl group of the *8Hq* and *8HqSH* molecules, were studied to get the adsorption geometries of the deprotonated species on the Al(111) surface. To study the adsorption of molecules on metallic surfaces in the framework of periodic calculations, it has been demonstrated that the same adsorption geometry has been obtained independently of the initial charge (anion/neutral radical) on the molecule [52–54].

An implicit solvent model was chosen to simulate the effect of water on the formation of the organic layer on Al(111). The VASPsol package [55,56] was used, with a relative permittivity of 78.4, which is the relative permittivity of water at ambient temperature.

Bader atomic net charges Q^{atom} were calculated from the values of electronic density using the program developed by the Henkelman group [57]. Net charge on an adsorbed species Q^{mol}_{ads} was obtained by summation of the bader atomic net charges on atoms of the adsorbed molecule.

Figs. 1,2, and 4 were plotted with the VESTA package [58,59].

From the results of the DFT calculations, the adsorption Gibbs energies in vacuum and the adsorption Gibbs energies of the molecules and of the deprotonated species from the aqueous phase were calculated as explained hereafter.

2.2.1. Adsorption Gibbs energies of the neutral species (molH and mol) on the Al(111) surface in vacuum

The adsorption Gibbs energy of a neutral species (*molH = 8Hq or 8HqSH*) or a radical (*mol = q, qSH* and *qS*), on the Al(111) surface was calculated in vacuum as:

$$G^{in\ vacuum}_{adsorption} = G^{\circ}(molH(or\ mol)on\ Al(111)) - \left(G^{\circ}(molH(or\ mol)) + G^{\circ}\left(Al(111)\right)\right) \quad (6)$$

With $G^{\circ}(molH(or\ mol)on\ Al(111))$ the Gibbs energy of the resulting system with a molecule (*molH (or mol)*) adsorbed on Al(111), $G^{\circ}(molH(or\ mol))$ the Gibbs energy of the isolated (*molH (or mol)*) species and $G^{\circ}(Al(111))$ the Gibbs energy of the bare relaxed aluminium surface. The Gibbs energies were calculated by the summation of electronic and zero-point energies. The values of the adsorption Gibbs energies in vacuum are presented in Table S2.

2.2.2. Adsorption Gibbs energies of neutral species (molH) from the aqueous phase

The adsorption of the neutral species from the aqueous phase was also simulated. To take into account the solvent (water) effects, a thermodynamic cycle was chosen as proposed by Kokalj *et al.* [60]. Values of the Gibbs energy were calculated and provided a more appropriate thermodynamic quantity instead of the values of the total energy *E*. Following this approach, the adsorption Gibbs energy for neutral species (*molH*) in aqueous phase $\Delta G^{in\ water}_{adsorption}(molH)$ was quantified from the adsorption Gibbs energy of the neutral molecule species $G^{in\ vacuum}_{adsorption}(molH)$ calculated in vacuum:

$$\Delta G^{in\ water}_{adsorption}(molH) = G^{in\ vacuum}_{adsorption}(molH) - \Delta G^{\circ}_{solvation}(molH) + \Delta\Delta G^{\circ}_{solvation}\left(molH//Al(111)\right) \quad (7)$$

With $\Delta G^{\circ}_{solvation}(molH)$ the solvation Gibbs energy of the neutral species (Table 1).

$\Delta\Delta G^{\circ}_{solvation}(molH//Al(111))$, currently named as differential adsorptive solvation Gibbs energy, was defined as:

$$\Delta\Delta G^{\circ}_{solvation}\left(molH//Al(111)\right) = \Delta G^{\circ}_{solvation}(molH\ on\ Al(111)) - \Delta G^{\circ}_{solvation}(Al(111)) \quad (8)$$

Where the two terms were the solvation Gibbs energies of the coated and bare Al(111) surfaces, respectively.

Concerning the calculation of $\Delta\Delta G^{\circ}_{solvation}$, it has been shown in the literature that the magnitude of this quantity is rather small for species adsorbed on Cu surfaces. For instance, values from −0.49 to +0.35 eV have been calculated for azole molecules adsorption on Cu(111) [52,54,60,61], on Cu(100) and on Cu(110) [52]. Therefore, the magnitude of $\Delta G^{in\ water}_{adsorption}(molH)$ is dominated by the competitive terms between the adsorption Gibbs energy calculated in vacuum $G^{in\ vacuum}_{adsorption}(molH)$ and the solvation Gibbs energy of the adsorbed species $\Delta G^{\circ}_{solvation}(molH)$. In our case, the $\Delta\Delta G^{\circ}_{solvation}(molH//Al(111))$ term (calculated values are presented in Table S3), was obtained using the solvation Gibbs energies $\Delta G^{\circ}_{solvation}$, calculated with the VASPsol package [55,56].

The following values were used for the adsorption of *8Hq* on Al(111): $G^{in\ vacuum}_{adsorption}(8Hq) = -1.44$ eV (Table S2), $\Delta G^{\circ}_{solvation}(8Hq) = -0.20$ eV (Table 1) and $\Delta\Delta G^{\circ}_{solvation}(8Hq//Al(111)) = -0.10$ eV (Table S3).

2.2.3. Dissociation of the neutral species (molH) on the Al(111) surface

The dissociation Gibbs energy, $G^{in\ water}_{dissociation}$, of the *8Hq* molecule on the Al(111) surface in presence of water was calculated by the equation:

$$G^{in\ water}_{dissociation} = G^{\circ}((q+H)on\ Al(111)) - G^{\circ}(8Hq\ on\ Al(111)) \quad (10)$$

With $G^{\circ}((q+H)\ on\ Al(111))$ the Gibbs energy of the most stable system with a *H* atom co-adsorbed with a *q* species. The naming "$(q+H)$ on Al(111)" has been chosen to represent the adsorbed species on Al (111) whatever their final net charge. $G^{\circ}(8Hq\ on\ Al(111))$ was the Gibbs energy of the system with a native *8Hq* molecule adsorbed on the aluminium surface, in presence of the implicit solvent model.

2.2.4. Adsorption Gibbs energies of charged species (mol^- and H^+) from the aqueous phase

The adsorption Gibbs energy of the deprotonated species *mol*$^-$, *i.e.* q^- and qSH^- species, was evaluated from the thermodynamic cycle proposed by Kokalj *et al.* [60]:

$$\Delta G^{in\ water}_{adsorption}(mol^-) = G^{in\ vacuum}_{adsorption}(mol) + AE - \Phi^* - \Delta G^{\circ}_{solvation}(mol^-) + \Delta\Delta G^{\circ}_{solvation}\left(mol//Al(111)\right) \quad (11)$$

With $G^{in\ vacuum}_{adsorption}(mol)$ the adsorption Gibbs energy of the neutral species (radical) calculated in vacuum (periodic calculations, values in Table S2), $\Delta G^{\circ}_{solvation}(mol^-)$ the solvation Gibbs energy of the charged species (in Table 1), and $\Delta\Delta G^{\circ}_{solvation}(mol//Al(111))$ the differential adsorptive solvation Gibbs energy (defined by Eq. (8), Table S3).

The following values were used for the adsorption of q^- on Al(111):

$G^{in\ vacuum}_{adsorption}(q) = -3.52 / -3.63$ eV (parallel/tilted geometries, Table S2), $\Delta G^{\circ}_{solvation}(q^-) = -2.87$ eV (Table 1) and $\Delta\Delta G^{\circ}_{solvation}(q//Al(111)) = -0.08$ eV (Table S3).

The following values were used for the adsorption of qSH^- on Al (111): $G^{in\ vacuum}_{adsorption}(qSH) = -3.99 / -3.74$ eV (parallel/tilted geometries, Table S2), $\Delta G^{\circ}_{solvation}(qSH^-) = -2.55$ eV (Table 1) and $\Delta\Delta G^{\circ}_{solvation}(qSH//Al(111)) = -0.64$ eV (Table S3).

AE was the adiabatic electron affinity calculated as:

$$AE = E^{in\ vacuum}_{tot}(mol) - E^{in\ vacuum}_{tot}(mol^-) \quad (12)$$

Values of 2.30 eV and 3.18 eV were obtained for the *q* and *qSH* species respectively.

Φ* was the work function of Al(111) with an adsorbed thick enough film of liquid water on it; a value of 3.31 eV was used, calculated as $\Phi^* = \Phi + \Delta\Phi$, with Φ the work function of the Al(111) bare surface (4.04 eV) and ΔΦ the work function change if the slab was covered by a film of liquid water (-0.73 eV).

The Gibbs adsorption energy of the proton H^+ was evaluated as:

$$\Delta G^{in\ water}_{adsorption}(H^+) = G^{in\ vacuum}_{adsorption}(H) - IP + \Phi^* - \Delta G^{\circ}_{solvation}(H^+) + \Delta\Delta G^{\circ}_{solvation}\left(H\middle//Al(111)\right) \quad (13)$$

With $G^{in\ vacuum}_{adsorption}(H)$ the adsorption Gibbs energy of the neutral species (radical) calculated in vacuum (periodic calculations), Φ* the work function of Al(111) with an adsorbed thick enough film of liquid water on it (3.31 eV), and $\Delta\Delta G^{\circ}_{solvation}(H//Al(111))$ the differential adsorptive solvation Gibbs energy (defined by Eq. (8)).

The following values were used for the adsorption of H^+on Al(111): $G^{in\ vacuum}_{adsorption}(H) = -2.56$ eV (Table S2) and $\Delta\Delta G^{\circ}_{solvation}(H//Al(111)) = -0.006$ eV (Table S3). A value of −11.53 eV was used for the absolute aqueous solvation free energy of the proton $\Delta G^{\circ}_{Solvation}(H^+)$ [45].

IP was the adiabatic ionisation potential calculated as:

$$IP = E^{in\ vacuum}_{tot}(H^+) - E^{in\ vacuum}_{tot}(H) \quad (14)$$

A value of 13.59 eV was obtained.

3. Experimental procedure: electrochemical measurements

The electrolytic solution (corrosive medium) was prepared from deionised water by adding 0.1 M Na_2SO_4 and a small concentration of chlorides (0.05 M NaCl) (reagent grade). The electrolyte was in contact with air at room temperature (20 °C ± 2°C). The pH of the blank solution was 6.5. *8Hq* and *8HqSH* were analytical grade reagents (purity = 99%) from Alfa Aesar and Sigma-Aldrich, respectively and were used as received. The concentration of *8Hq* (3×10^{-3} M) was chosen near its solubility limit in neutral solution. The same concentration was chosen for the *8HqSH*. The addition of the *8HqSH* in the electrolyte led to a pH decrease (pH = 3 for a concentration of 3×10^{-3} M). In order to compare the mode of action of the two compounds, the pH of the corrosive medium containing the *8HqSH* was adjusted at a value of 6.5 by a 0.1 M NaOH solution. The electrochemical experiments were carried out with a pure Al (99.9999 wt%) rod provided by Praxair, with a cross-sectional area of 1 cm^2. The body of the rod was covered with a heat-shrinkable sheath, leaving only the tip of the rod in contact with the electrolyte. The samples were abraded with successive SiC papers (grade 1200) then cleaned in ethanol in an ultrasonic bath and finally dried in warm air.

A three-electrode cell was used for the electrochemical measurements with a platinum grid counter-electrode, a saturated calomel reference electrode (SCE) and the pure Al rod as working electrode (rotating disk). The rotation rate was fixed at 500 rpm. Open Circuit Potential (OCP) variation, polarisation curves and electrochemical impedance measurements were obtained using a Biologic VSP apparatus. The anodic and the cathodic parts of the polarization curves were obtained separately from the OCP at a potential sweep rate of 0.6 V/h. Impedance diagrams were acquired at the OCP over a frequency range of 65 kHz to a few mHz with eight points per decade using a 20 mV peak-to-peak sinusoidal voltage. The polarisation curves and the impedance diagrams are shown after 20 h of immersion at the OCP.

4. Results and discussion

The *8Hq* molecule and its derivatives are presented in Fig. 1. The pKa values corresponding to the hydroxyquinoline OH group are 9.89 and 8.66 for the *8Hq* [62] and the *8HqSH* [63] molecules respectively, leading to protonated/deprotonated species depending of the pH of the aqueous solution. The experiments were performed at pH = 6.5, and the native *8Hq* and *8HqSH* forms were then the most abundant species in solution. However, deprotonated molecules q^- and qSH^- were also present, even in very low concentration. As it has been shown in previous works [22–26], these latter forms led to the strongest interaction with aluminium during the formation of complexes, in solution or on the aluminium surface and they were also studied numerically.

The pKa of the SO_3H/SO_3^- group in these molecules has been calculated at a value of −4.9 by Le Bahers *et al.* [64]. Thus, the sulfonic group of the molecule was mostly deprotonated in aqueous solution at pH = 6.5 and the qS^{2-} species was also studied theoretically. As the neutralisation of the SO_3^- group by a cationic species present in the aqueous solution (Na^+, for example) is highly probable, it was also simulated in this work taking the qSH^- species as a model of the neutralised species [65,66].

In the following, results of DFT calculations are first presented. These investigations at atomic scale, including a solvent model, are useful to reveal differences between the two *8Hq* and *8HqSH* molecules and their deprotonated species in interaction with Al^{3+} cations or Al(111) surfaces. The electrochemical measurements (polarisation curves and impedance spectroscopy) performed on pure aluminium during immersion in a neutral aqueous solution in the presence of the two quinoline derivatives allowed in a second step their inhibitive properties to be characterised.

4.1. DFT results

The alkoxide species of the quinoline molecules, deprotonated on the hydroxyl group, are denoted q^-, qSH^- and qS^{2-} and their complexes with Al^{3+} cations are denoted Alq_3, $Al(qSH)_3$ *and* $Al(qS)_3^{3-}$, hereafter. Two isomers may exist for the complexes, the meridional and the facial one [67,68]. The *mer* isomers are shown in Fig. 2 and were the only isomers studied in the current computations because they have been experimentally identified in solution [67,68].

4.1.1. Native molecules, complexes, and their deprotonated species in aqueous phase

The calculation of molecular electronic properties, such as the HOMO and LUMO energies (ε_{HOMO} and ε_{LUMO}) and the HOMO/LUMO gap, defined as ($\varepsilon_{LUMO} - \varepsilon_{HOMO}$), that could be relevant to the understanding of inhibition mechanisms by organic compounds has been the purpose of several review papers [14,15,69]. However, it has been demonstrated that this approach cannot be directly related to corrosion inhibition [16,17]. Studying the frontier orbital energies and HOMO-LUMO gap of the molecules in vacuum or in water might be helpful but doing so without considering others aspects would not respond to the complex problem of corrosion inhibition mechanisms.

Among the factors contributing to corrosion inhibition, the solvation of inhibitors candidates seemed first of all of great importance: a strong solvation favours the stability of hydrated inhibitors in the aqueous solution and thus, could decrease the adsorption affinity of the molecules with the metal surface. The solvation Gibbs energies $\Delta G^{\circ}_{Solvation}$ at 298.15 K in water, for the native molecules, complexes and for their

Table 1
Solvation Gibbs energies at 298.15 K for the free molecules and anions (in eV).

Species	*8Hq*	*8HqSH*	*8HqS*$^-$	*q*$^-$	*qSH*$^-$	*qS*$^{2-}$
$\Delta G^{\circ}_{Solvation}$	-0.20	-0.54	-2.62	-2.87	-2.55	-8.07

Table 2
Solvation Gibbs energies at 298.15 K for the aluminium complexes (in eV).

Species	*Al(q)*$_3$	*Al(qSH)*$_3$	*Al(qS)*$_3^{3-}$
$\Delta G^{\circ}_{Solvation}$	-0.47	-1.47	-34.65

deprotonated species, are reported in Tables 1 and 2. If we compare the free native *8Hq* and *8HqSH* molecules, at 298.15 K, the latter molecule has the strongest solvation Gibbs energy (-0.54 eV). This is a first indication of an easier solubilisation in water of the *8HqSH* compared to the native *8Hq* molecule. The solvation Gibbs energy of *8HqS*$^-$ is −2.62 eV. This anionic species is strongly stabilised in solution, and it is also the case for all the anionic species that are highly solvated with more exothermic solvation Gibbs energies than for the native forms. The most charged anions, *qS*$^{2-}$ and *Al(qS)*$_3^{3-}$ have the strongest solvation Gibbs energies. But it must be underlined that the calculated values for these two latter species are raw approximations because Truhlar and co-workers' SMD model is applicable to uncharged and monocharged solutes in water [45] but has not been parametrised on multi-charged species. Overall, the addition of the *SO*$_3$*H* group on the *8Hq* and the *q*$^-$ species increased the exothermic character of the solvation. The hydrated species in solution are thus very stable and this could be detrimental to the adsorption of the sulfonic/sulfonate species on the metal surface.

The solvation Gibbs energy, combined to the vapour pressure of a molecule, allows its solubility in water to be calculated (Eq. (5)). It then comes:

$$\frac{s(8HqSH)}{s(8Hq)} = 4.82\ 10^5 \times \frac{P^{\circ}_{8HqSH}}{P^{\circ}_{8Hq}} \quad (15)$$

The vapour pressure at 298 K is available for the *8Hq* molecule (P°_{8Hq}= 1.6 10^{-3} mm Hg [70]), but it is not the case for the *8HqSH* species. The values that are available in the literature for *8Hq* derivatives, *i.e.* 5-nitro-8-hydroxyquinoline and 2-methyl-8-hydroxyquinoline [71] and halogen-modified 8-hydroxyquinolines [72], are lower at 298 K than the vapour pressure of native *8Hq*. Concerning the sulfonic species, the vapour pressure of benzene sulfonic acid and p-hydroxy benzene sulfonic acid are respectively 2.36 10^{-5} mm Hg and 3.33 10^{-7} mm Hg at 298 K [73]. Thus, we can estimate from Eq. (15) that the solubility of *8HqSH* in water is more than one hundred times higher than the solubility of *8Hq*. This is a first aspect to take into account to study molecules / metal surfaces interactions in aqueous solution.

A study of the formation of complexes between the deprotonated inhibitor molecules and one Al^{3+} cation was needed in relation with Al dissolution. The complexation Gibbs energies of the aluminium complexes were calculated and converged toward −22.72 ± 0.31 eV in water. These values related to the naked Al^{3+} cation are very strong and largely overestimated because hydrated Al^{3+} is more stable as $[Al(H_2O)_6]^{3+}$ [74]. The $[Al(H_2O)_6]^{3+}$ complex would be a more accurate model of solvated Al^{3+} than the bare Al^{3+} ion and an implicit solvent model. However, the small range of data (± 0.31 eV) of the values showed similar chelating properties for the three deprotonated species. The addition of the *SO*$_3$*H* group did not significantly modify the complexation Gibbs energies of the Al^{3+} cation with three *q*$^-$, or *qSH*$^-$ or *qS*$^{2-}$ anions. The solvation Gibbs energies for the complexes at 298.15 K are presented in Table 2. In all the cases, the solvation of the molecules stabilised the systems (-0.47 and −1.47 eV for *Al(q)*$_3$ and *Al(qSH)*$_3$) and the sulfonic/sulfonate species were the most solvated ones. Again, the value calculated for the *Al(qS)*$_3^{3-}$ complex has to be taken into account only qualitatively.

Similarly to the quinoline molecules and anions, the *Al(qSH)*$_3$ and *Al(qS)*$_3^{3-}$ species appeared strongly solvated in the aqueous phase. This could be unfavourable to their adsorption on the metal surface. This is a first difference in the chemical behaviour of the *8Hq* and *8HqSH* molecules. However, there will be anyway a small concentration of native and deprotonated molecules in solution that can interact with the aluminium surface. The adsorption of the molecules on the Al(111) surface is thus presented in next section.

4.1.2. Adsorption of deprotonated species q$^-$, qSH$^-$ and qS^{2-} on Al(111) from aqueous phase

The study of organic molecules adsorption on the metal substrate is today recognised as a mandatory step to investigate the inhibitors efficiency. It could lead to a dissociative adsorption of the inhibitor on the metallic surface. The question of the O-H bond breaking in the hydroxyquinoline molecule had therefore to be considered by the study of the O-H bond dissociation on the Al(111) surface, in presence of water. The chemisorption and dissociation processes that can occur on the Al(111) surface for the *8Hq* molecule are reviewed in Fig. 3.

In the present computations (implicit solvent model), the dissociation Gibbs energy of the free *8Hq* species in water is 1.29 eV and it is thus endothermic (Fig. 3(a) and section S4). The adsorption Gibbs energies on Al(111) are −1.34 eV, −1.85 eV and −1.32 eV for the most stable adsorption geometries of (*8Hq* on Al(111)), (*q* on Al(111)) and (*H* on Al(111)) (Fig. 3(b), (c) and (d), respectively). When the species, coming from the aqueous phase, were co-adsorbed on Al(111), the adsorption Gibbs energy is −3.14 eV ((*q*+*H* on Al(111)) in Fig. 3(e)). In the latter system, the distance between the deprotonated species and the *H* atom co-adsorbed is 5.593 Å. From a thermodynamic point of view, the dissociation of *8Hq* is exothermic on Al(111) with a dissociation energy of −0.45 eV and a dissociation Gibbs energy of −0.52 eV in presence of water (Fig. 3(f)). Regarding this low energetic value, it can be reasonably considered that the activation energy for the dissociation on the surface should have a low value and thus, it can be concluded that deprotonated species are predominant on the Al(111) surface.

To complement the process of the adsorption and dissociation of *8Hq* species on the bare Al(111) surface from the aqueous phase, the adsorption and dissociation of *8Hq* molecules were investigated in presence of surface *O* or *OH* species, always present on the Al(111) surface. To that aim, the following deprotonation reactions on (i) the O_{ads}/Al(111) and (ii) the OH_{ads}/Al(111) surfaces were considered: $8Hq_{ads} + O_{ads}/Al(111) \xrightarrow{(i)} q_{ads} + OH_{ads}/Al(111)$ and $8Hq_{ads} + OH_{ads}/Al(111) \xrightarrow{(ii)} q_{ads} + H_2O_{ads}/Al(111)$. The results showed that the dissociation process of *8Hq* on O_{ads}/Al(111) is endothermic (reaction Gibbs energy of (*i*) = +0.34 eV) and the presence of the O species on the Al(111) surface does not promote the dissociation of the *8Hq* molecule on the metal surface. The dissociation process of *8Hq* on OH_{ads}/Al(111) is exothermic (reaction Gibbs energy of (*ii*) = −0.19 eV) but the dissociation process on the bare Al(111) surface is more favoured (-0.52 eV). This trend is similar if the *8Hq* free molecule is taken in the initial state of the process instead of the $8Hq_{ads}$ one.

The most stable adsorption geometries of the molecules on the Al(111) surface with the implicit solvent model are presented in Fig. 4 (and selected geometrical parameters are presented in Table S5). The adsorption geometries, of the *q*, *qSH* and *qS* species modelling the deprotonated molecules, were a parallel mode relatively to the Al(111) surface or a tilted mode as it was already the case in our previous computations in vacuum [25]. For the tilted geometries, adsorbed species are bounded to the Al(111) surface by their O and N atoms. The O atom is in bridge position on the Al(111) surface and the two O-Al shortest distances are respectively in the range of 1.901–1.910 Å and 2.005–2.036 Å, whereas the N atom is on-top of an Al atom with a N-Al distance of 2.027–2.036 Å. The tilt angle α between the adsorbed

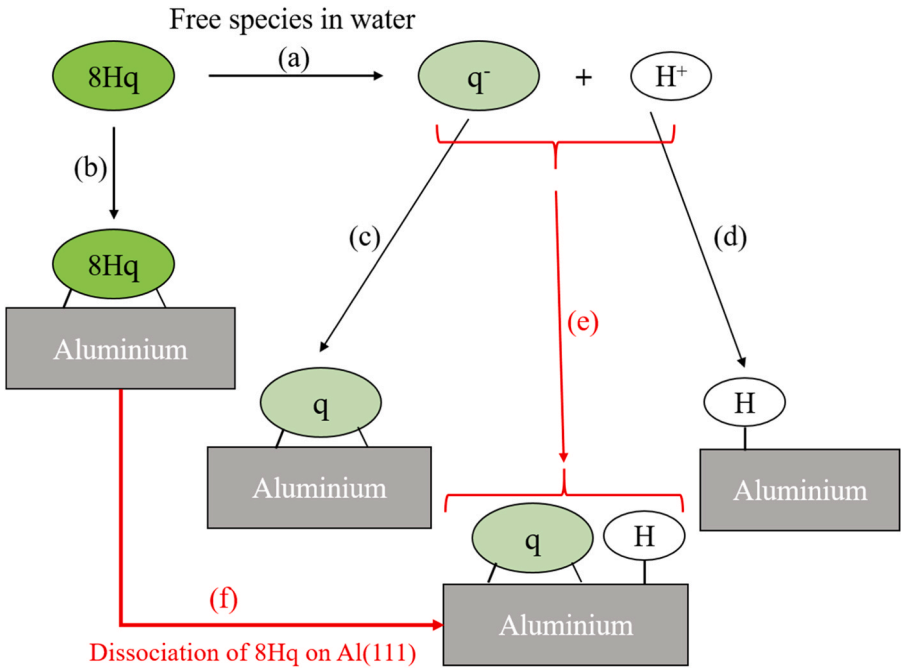

Fig. 3. Chemisorption and dissociation processes for *8Hq* in presence of water. (a): dissociation of *8Hq*; (b): chemisorption of *8Hq* on Al(111); (c): chemisorption of *q* on Al(111); (d): chemisorption of *H* on Al(111); (e): co-adsorption of *q* and *H* on Al(111); (f): dissociation of *8Hq* on Al(111); the charge on the adsorbed species is not mentioned in the Figure.

molecules and the Al(111) surface has a value ranging from 57.0 to 69.6°. For the parallel conformations (α = 9.7–12.3°), the O and N atoms are on-top of an Al surface atom ($d_{O\text{-}Al}$ from 1.813 to 1.831 Å and $d_{N\text{-}Al}$ from 1.918 to 1.924 Å). A bond is also formed between one carbon of the pyridine cycle and one Al atom of the surface ($d_{C\text{-}Al}$ from 2.188 to 2.203 Å). Additionally, for the *qSH* and *qS* adsorbed species, two of the O atoms of the SO_3H/SO_3 group are bounded to the Al surface (with bond lengths between 1.954 and 2.189 Å).

The adsorption Gibbs energies of the deprotonated species were calculated and are given in Table 3. From the most stable geometries, it comes: $\Delta G^{in\ water}_{adsorption}(q^-) - \Delta G^{in\ water}_{adsorption}(qSH^-) = 0.12$ eV. This positive value shows that qSH^- is more strongly adsorbed on Al(111) that the q^- species. In more details, it is more strongly adsorbed on the Al(111) surface than the q^- molecule, both in tilted and parallel conformations. However, the tilted geometry is the most stable one for the q^- molecule whereas the parallel conformation is the most stable one for the qSH^- and qS^{2-} species. For the latter one, it was not possible to determine the most stable geometry for the free *qS* molecule, modelling qS^{2-} species, due to non-realistic geometry of the SO_3 group. Thus, the adsorption Gibbs energies from the aqueous phase could not be accurately calculated but the parallel conformation is more stable of 1.82 eV than the tilted one. Nevertheless, an evaluation of the adsorption energy was done using the energy of a geometry optimised with a constraint on the S-O bond lengths of the SO_3 group for the free molecule (Adsorption energies: −6.58 eV and −6.16 eV in vacuum and in water, respectively for the radical species). However, calculation of $\Delta G^{in\ water}_{adsorption}(qS^{2-})$ with sufficient precision could not be possible (see section S6 for the calculation attempt).

The preferred parallel conformation for the adsorbed sulfonic and sulfonate molecules over the tilted one can be explained by the additional bonds formed between the O atoms of the SO_3H/SO_3 group and the Al surface atoms. The addition of the SO_3H or SO_3 group increases the strength of the bonding of the inhibitor on the Al(111) surface. The iono-covalent character of the bonding between the molecules and the Al(111) surface can be deduced from the electronic density shown in Fig. 4 (accumulation of the electronic density between atoms of the molecules and the Al surface) and the electron transfers from the metal surface to the adsorbed species (Table 3) for the parallel geometries (1.06–1.24 electrons).

From the DFT computations, the following points can be emphasised:

(i) The negative values of the solvation Gibbs energies ($\Delta G^{\circ}_{Solvation}$ at 298.15 K) for the native *8Hq* molecule and the $Al(q)_3$ complexes show an exothermic process and agree well with the qualitatively known experimental solubilisation of these species in water.
(ii) The adsorption of the *8Hq* molecules on the Al(111) surface, followed by its deprotonation, is thermodynamically favoured.
(iii) The deprotonated species are strongly adsorbed on the metal surface which could lead to the formation of a layer on the aluminium surface. The layer would be composed of stand-alone molecules or complexes on the surface. This is in favour of the corrosion inhibition process.
(iv) The aluminium complexes with the *8HqSH* species are highly soluble in solution, more soluble than the aluminium complexes with the *8Hq* molecules, *i.e.* $Al(q)_3$. This might lead to aluminium dissolution and thus, might accelerate the corrosion process.

To complement these calculations, electrochemical measurements were performed to go further.

4.2. Electrochemical results

Fig. 5 illustrates the OCP variation of the Al electrode in the electrolytic solution (blank solution), with the *8Hq* and the *8HqSH* molecules. For the three electrolytes (with and without the organic molecules), when the Al sample was dipped in the electrolyte, the OCP values are similar, around −0.92 V/SCE. This indicates that the initial surface condition is identical and the measurements start with the same reference state. During the first 2 h of immersion, regardless of the system, the OCP evolves towards cathodic potentials. This variation in the cathodic direction is more pronounced with the *8HqSH*. In the presence of the *8HqSH*, the OCP continues to evolve slowly in the cathodic direction when the immersion time increases and it reaches a

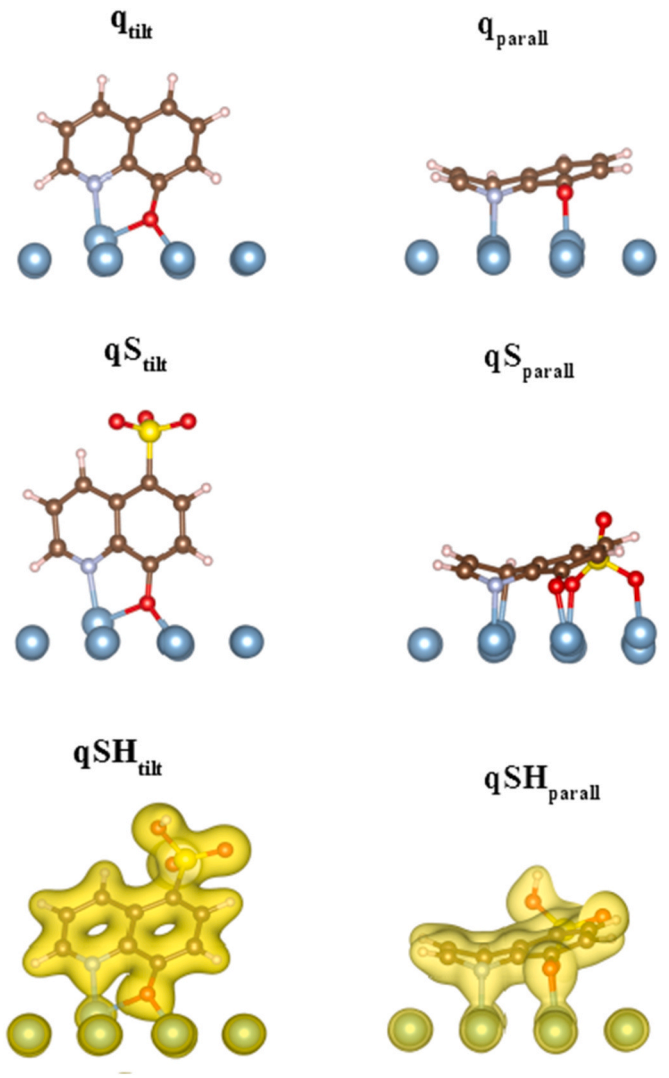

Fig. 4. (*q* on Al(111)), (*qS* on Al(111)) and (*qSH* on Al(111)) in presence of water; left: tilted geometries; right: parallel geometries; atom colour code: *C*: brown balls, *N*: small blue balls, *S*: yellow ball, *H*: white balls, *Al*: big blue balls; for the *qSH* species, the electronic density on the system is also plotted in yellow (ρ=0.051 electrons/Å^3).

Table 3
Adsorption geometries, adsorption Gibbs energies $\Delta G^{in\ water}_{adsorption}$ and net charges on the molecules adsorbed on Al(111).

Species	q^-		qSH^-		qS^{2-}	
Adsorption geom.	parallel	tilted	parallel	tilted	parallel	tilted
$\Delta G^{in\ water}_{adsorption}$ (eV)	-1.74	-1.85	-1.97	-1.72	Most stable of 1.82 eV	/
Q^{mol}_{ads} (e)	-2.06	-1.00	-2.24	-1.15	-3.11	-1.95
ΔQ^{mol*}_{ads} (e)	-1.06	0.0	-1.24	-0.15	-1.11	+0.05

$\Delta Q^{mol*}_{ads} = Q^{mol}_{ads} - Q^{free\ mol}_{in\ water}$

stationary value, around −1.15 V/SCE, after 6–8 h of immersion. Without inhibitor and with the *8Hq* and after 2 h of immersion, the shape of the OCP curves is quite similar: OCP increases with time and tends to stabilize after approximatively 20 h of immersion. This type of variation is often associated with the formation of protective films (organic or passive layers [7]). In the presence of the *8Hq*, the OCP value

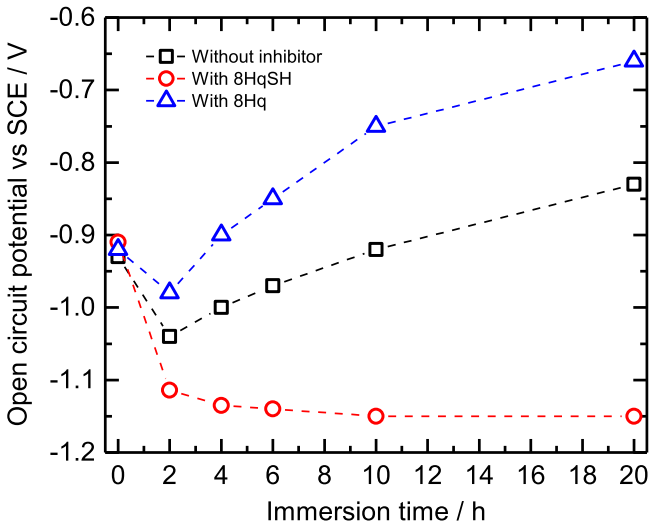

Fig. 5. Open circuit potential (OCP) of pure Al as a function of immersion time in a 0.1 M Na_2SO_4 + 0.05 M NaCl solution (pH = 6.5): without inhibitor, with *8Hq* and with *8HqSH*; electrode rotation rate: 500 rpm.

is more markedly shifted in the anodic range (+0.2 V/SCE) by comparison with the blank solution. Due to the OCP variation, polarisation curves and impedance diagrams are shown after 20 h of immersion.

4.2.1. *Polarisation curves*

Fig. 6 compares the polarisation curves obtained on pure Al for the blank solution (without inhibitor), with the *8Hq* and with the *8HqSH*. The corrosion potential is strongly influenced by the presence of the molecules, as already seen in Fig. 5. After 20 h of immersion, a corrosion potential difference of about 0.5 V is observed for the Al electrode in the presence of each molecule. In the cathodic domain, with and without inhibitors, the increase of the current densities with the overpotential is due to the oxygen reduction reaction. Then, at around −1.2 V/SCE, reduction of water also occurs producing an additional cathodic current increase. With *8HqSH*, the oxygen reduction reaction is not observed because the corrosion potential is around −1.2 V/SCE and the cathodic reaction, from this potential value, is mainly the water reduction. Near the corrosion potential, the cathodic current densities are higher in the

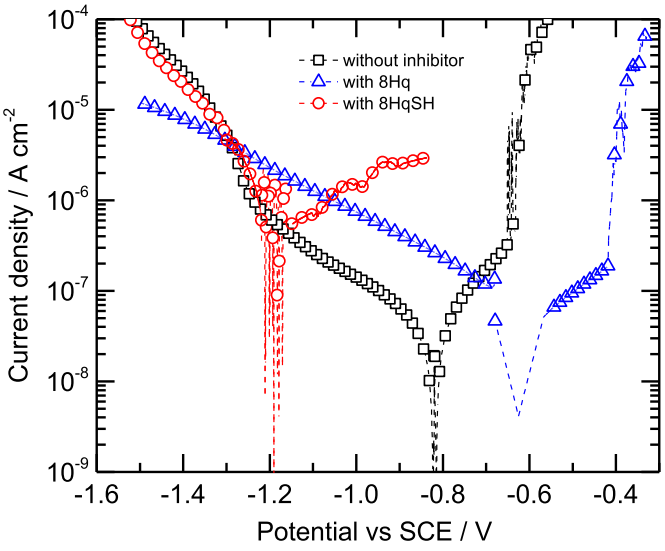

Fig. 6. Polarisation curves obtained on pure Al after 20 h of immersion in a 0.1 M Na_2SO_4 + 0.05 M NaCl solution (pH = 6.5): without inhibitor, with *8Hq* and with *8HqSH*; electrode rotation rate: 500 rpm.

presence of *8Hq* compared to the blank solution. In the anodic domain, the curves account for the aluminium dissolution and/or for the formation of an oxide film on the Al surface. In the presence of *8HqSH*, oscillations are observed in the whole anodic range (the curve superimposed to the data is a smoothed version of all the data points) and the current densities are rather high ($> 10^{-6}$ A cm^{-2}). Without inhibitor and with *8Hq*, the anodic current densities are low (below 10^{-6} A cm^{-2}) between the corrosion potential and −0.6 and −0.4 V/SCE, respectively. Then, an abrupt increase of the anodic current densities is observed when the potential increases due to the breakdown of the oxide film and/or to the development of pits. This result stresses again that the two compounds act differently. With *8Hq*, the polarisation curve looks the same as the curve without inhibitor but with higher cathodic current densities and lower anodic current densities. The anodic part indicates the presence of a film (oxide and/or oxide + *8Hq*). The shift of the corrosion potential in the anodic direction in the presence of *8Hq* is caused by the increase of the cathodic current densities. With *8HqSH*, the anodic curve reflects the absence of protective film, consistent with a corrosion potential value strongly shifted towards a very negative value by comparison with the Al for the blank solution.

4.2.2. Impedance diagrams

The impedance diagrams obtained on pure aluminium after 20 h of immersion in the neutral solution without inhibitors, with *8Hq* and with *8HqSH* are shown in Fig. 7. In the absence of inhibitor and with *8HqSH*, the diagrams present only one time constant which characterises the oxide film and the oxygen reduction reaction on the passive layer [9,27]. The values of the impedance modulus at low frequency is about ten times lower in the presence of *8HqSH* compared to the blank solution. This indicates that the corrosion rate of aluminium increases in the presence of this molecule and the shape of the diagram (both impedance modulus and phase angle) suggests that the oxide film would be thinner than without inhibitor. In the presence of *8Hq*, the impedance modulus is little modified, slightly higher, by comparison with the blank solution, whereas two time constants are visible on the phase angle. The first time constant in the high frequency range might be linked to the formation of a protective layer composed of insoluble aluminium complexes [7] while the low frequency part of the diagram characterises the aluminium oxide layer and the oxygen reduction [9,27]. The shape of the impedance diagrams emphasizes once more that *8Hq* and *8HqSH* have different effects at the Al/electrolyte interface.

In recent papers, it has been shown that, from the impedance data, it was possible to obtain information on the interfacial properties. Particularly, in the case of oxide or organic films, the capacitance of the layers (C_{ox} or C_{film}) can be extracted by using the complex-capacitance representation, without using any model [28,30]:

$$C(\omega) = \frac{1}{j\omega[Z(\omega) - R_e]} \tag{16}$$

With $\omega = 2\pi f$ and R_e, is the electrolyte resistance.

Fig. 8 presents the complex-capacitance plots for the pure Al in the electrolyte without inhibitor and with the two compounds. The comparison of the complex capacitance plots shows that the high frequency part is rather similar for the Al without inhibitor and in the presence of the *8HqSH* but, on the contrary, the curve obtained in the presence of the *8Hq* is different. Capacitance values, determined by extrapolation of the high-frequency data to the real axis, are reported in Table 4. The value obtained without inhibitor (around 5 μF cm^{-2}) is lower than that obtained in the presence of the *8HqSH* (around 8 μF cm^{-2}). Then, the thickness of the aluminium oxide film, δ_{ox}, can be calculated from the relationship:

$$\delta_{ox} = \frac{\varepsilon_{ox}\varepsilon_0}{C_{ox}} \tag{17}$$

where ε_{ox} is the dielectric permittivity of Al_2O_3 ($\varepsilon_{ox} = 10$) and ε_0 is the vacuum permittivity.

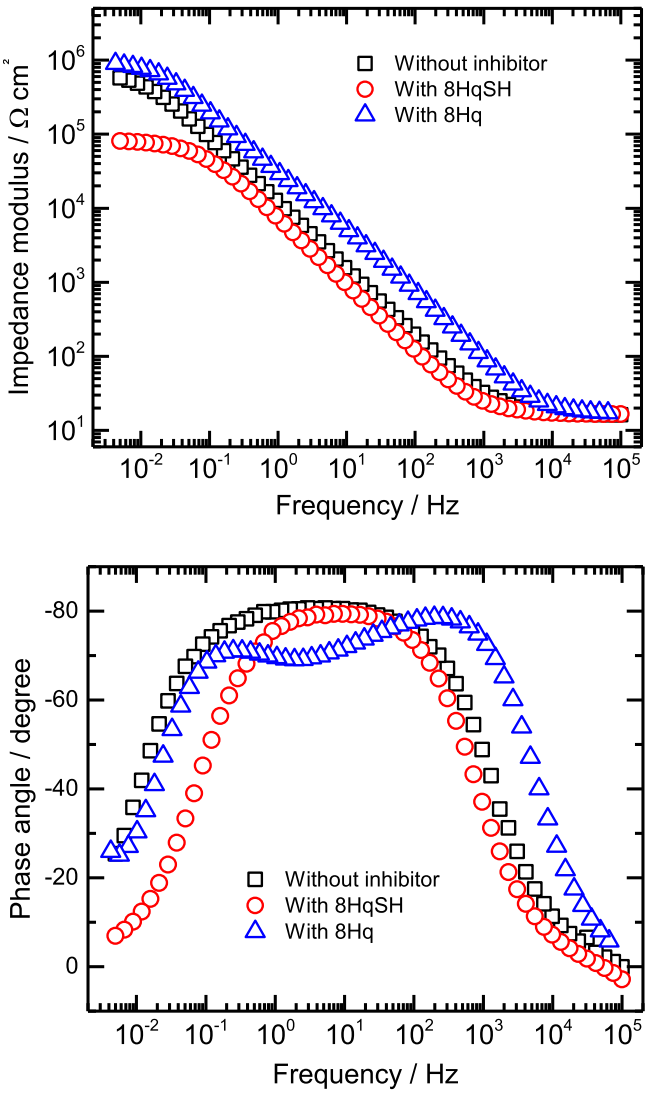

Fig. 7. Electrochemical impedance diagrams (Bode plots) obtained on pure aluminium after 20 h of immersion at E_{corr} in a 0.1 M Na_2SO_4 + 0.05 M NaCl solution: without inhibitor, with *8Hq* and with *8HqSH*; electrode rotation rate: 500 rpm.

In the presence of the *8Hq*, it is possible to extract a film capacitance value around 1.4 μF cm^{-2}. In that case, the capacitance at high frequency cannot be attributed to an oxide layer (the thickness would be too high) and thus, it accounts for the presence of *8Hq* molecules or aluminium complexes on the Al surface. The thickness of this film can be estimated from the same relationship as for the oxide film but in that case, the dielectric permittivity of the *8Hq* must be taken into account in Eq. (17) ($\varepsilon_{8Hq} = 2$). The oxide film and the protective film thicknesses calculated from the impedance data are reported in Table 4. Even if the values could not be accurately determined, the films thickness can be compared. It was shown that the oxide film formed on the Al surface without inhibitor is about 2 nm and it is significantly thinner (1 nm) in the presence of the *8HqSH*. With the *8Hq*, there is the formation of a layer driven by the interactions of the *8Hq* and the aluminium oxide layer, most probably as Al complexes.

On the basis of the electrochemical results, the following points can be emphasised:

(i) Without inhibitor, during immersion in aqueous solution, the corrosion of aluminium leads to the formation of an oxide layer.

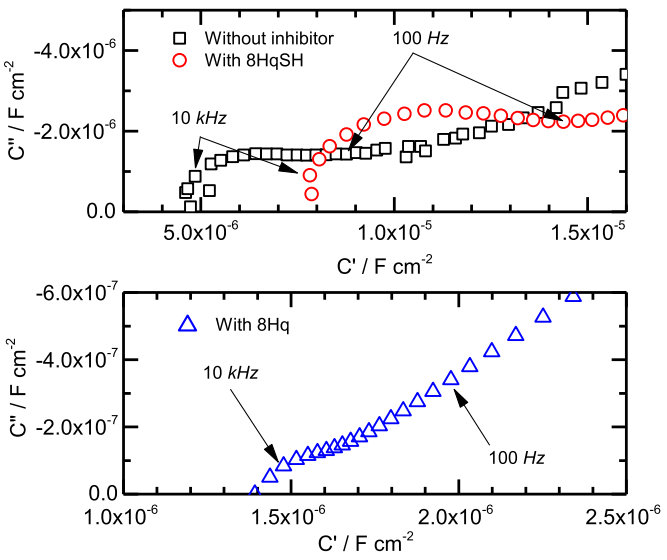

Fig. 8. Complex capacitance plots corresponding to the EIS spectra (corrected from the electrolyte resistance) in Fig. 7.

Table 4
Capacitance values obtained from the complex-capacitance plots at C'' = 0 (Fig. 8). Oxide film and protective film thicknesses calculated according to Eq. (17) without inhibitor, with *8HqSH* or with *8Hq*.

	C_{ox} ($\mu F\ cm^{-2}$)	C_{film} ($\mu F\ cm^{-2}$)	ε Al_2O_3	ε *8Hq*	δ_{ox} (nm)	δ_{film} (nm)
Without inhibitor	4.8	/	10	/	1.8	/
With *8HqSH*	7.8	/	10	/	1.1	/
With *8Hq*	/	1.4	/	2	/	1.3

Its thickness after 20 h of immersion in the electrolyte was estimated at 2 nm. The insulating character of the oxide film limits the oxygen reduction reaction. This explains the low cathodic current densities (0.01–1 $\mu A\ cm^{-2}$). The anodic polarisation curve also accounts for the presence of an oxide film according to low current densities and a potential breakdown for higher anodic potential values.

(ii) With *8HqSH*, the impedance result indicates the presence of an oxide layer, the thickness of which is lower than that formed in the blank solution. The fluctuations of the anodic current densities observed on the polarisation curve would be indicative of the dissolution of the oxide layer linked to the solubility of the complexes, formed between the molecules and the Al^{3+} cations. At the corrosion potential, for which EIS measurements were performed, the competition between complexes formation and dissolution would be in favour of the oxide film. When the dissolution proceeds via the anodic polarisation, the formation of complexes increases the dissolution rate. This is in agreement with the corrosion potential value, strongly shifted towards cathodic values (-1.2 V/SCE) which corresponds to an almost bare aluminium surface.

(iii) With *8Hq*, the same mechanism would be involved with the formation of complexes with the Al^{3+} cations. But, in that case, their solubility is limited and a protective layer is formed above the oxide layer. Its thickness was estimated around 1.2 nm. The formation of this layer impedes the growth of the oxide film. This explains why the cathodic current densities were higher.

5. Conclusions

In our previous works, the bonding of the molecules on bare Al(111) surfaces, and on oxidised and hydroxylated aluminium surfaces has been investigated [22–26]. We considered in the present work the presence of water on the strength of this bonding. Computational and electrochemical experimental approaches were combined with the goal to find descriptors correlated to the inhibitor efficiency.

For the *8Hq* molecule and its sulfonic and sulfonate derivatives, the results of the DFT studies first showed that, even if it was not possible to calculate the solubility of *8HqSH*, the strong solvation Gibbs energies of the sulfonic and sulfonate species indicated a strong tendency to solubilisation in water, with a solubility evaluated one hundred times higher than the solubility of *8Hq*. Moreover, the aluminium complexes with the *8HqSH* species were much more soluble in aqueous solution than the complexes with the *8Hq* molecules. DFT computations of adsorption Gibbs energies on the adsorption of the deprotonated molecules on Al(111), in presence of water, revealed that all the quinoline species were strongly adsorbed on the aluminium surface with a favoured formation of an organic layer on the surface, as stand-alone molecules or Al complexes.

The electrochemical results obtained with the two molecules clearly showed different behaviours of the molecules on the Al surface. With the *8Hq*, the presence of a protective film on the pure Al surface is confirmed, most likely composed of aluminium complexes with the organic molecules. The film thickness was in the range 1–2 nm. The film formation would be favoured by the anodic and cathodic reactions: the oxygen reduction produces OH^- ions which generate the q^- species and these species would react with the Al^{3+} produced by the anodic dissolution. *8Hq* is an effective corrosion inhibitor. In the presence of *8HqSH*, there was no protective film formed on the aluminium surface and in contrast, these molecules accelerate the aluminium dissolution by the solubilisation of *8HqSH* complexes in agreement with the DFT computations that show the high solvation of these species in solution. This is a key factor which controls the action of the investigated molecules on the Al surface.

Funding

This work was supported by the French Ministry of Higher Education and Research [Y.B., PhD grant] and has been granted access to the HPC resources of CALMIP supercomputing center under the allocation [p12174].

CRediT authorship contribution statement

Yann Bulteau: Investigation. **Nadine Pébère:** Writing – review & editing, Supervision, Data curation, Conceptualization. **Corinne Lacaze-Dufaure:** Writing – review & editing, Supervision, Software, Project administration, Funding acquisition, Data curation, Conceptualization. **Fatah Chiter:** Investigation. **Pierre Bonin:** Investigation.

Declaration of Competing Interest

The authors declare that they have no known competing financial interests or personal relationships that could have appeared to influence the work reported in this paper.

Data Availability

Data will be made available on request.

Appendix A. Supporting information

Supplementary data associated with this article can be found in the online version at doi:10.1016/j.corsci.2024.112104.

References

[1] M. Albrecht, M. Fiege, O. Osetska, 8-Hydroxyquinolines in metallo-supramolecular chemistry, Coord. Chem. Rev. 252 (2008) 812–824, https://doi.org/10.1016/j.ccr.2007.06.003.

[2] F.C.F. Barros, F.W. Sousa, R.M. Cavalcante, T.V. Carvalho, F.S. Dias, D.C. Queiroz, L.C.G. Vasconcellos, R.F. Nascimento, Removal of copper, nickel and zinc ions from aqueous solution by chitosan-8-hydroxyquinoline beads, Clean. (Weinh. 36 (2008) 292–298, https://doi.org/10.1002/clen.200700004.

[3] M.L. Ramos, L.L.G. Justino, A.I.N. Salvador, A.R.E. de Sousa, P.E. Abreu, S. M. Fonseca, H.D. Burrows, NMR, DFT and luminescence studies of the complexation of Al(III) with 8-hydroxyquinoline-5-sulfonate, Dalton Trans. 41 (2012) 12478–12489, https://doi.org/10.1039/c2dt31381b.

[4] C.W. Tang, S.A. Van Slyke, Organic electroluminescent diodes, Appl. Phys. Lett. 51 (1987) 913–915, https://doi.org/10.1063/1.98799.

[5] Z. Shen, P.E. Burrows, V. Bulovic, S.R. Forrest, M.E. Thompson, Three-color, tunable, organic light-emitting devices, Science 276 (1997) 2009–2011, https://doi.org/10.1126/science.276.5321.2009.

[6] V. Prachayasittikul, S. Prachayasittikul, S. Ruchirawat, V. Prachayasittikul, 8-Hydroxyquinolines: a review of their metal chelating properties and medicinal applications, Drug Des. Devel. Ther. 7 (2013) 1157–1178, https://doi.org/10.2147/DDDT.S49763.

[7] L. Garrigues, N. Pébère, F. Dabosi, An investigation of the corrosion inhibition of pure aluminum in neutral and acidic chloride solutions, Electrochim. Acta 41 (1996) 1209–1215, https://doi.org/10.1016/0013-4686(95)00472-6.

[8] S. Lamaka, M. Zheludkevich, K. Yasakau, M. Montemor, M. Ferreira, High effective organic corrosion inhibitors for 2024 aluminium alloy, Electrochim. Acta 52 (2007) 7231–7247, https://doi.org/10.1016/j.electacta.2007.05.058.

[9] S. Marcelin, N. Pébère, Synergistic effect between 8-hydroxyquinoline and benzotriazole for the corrosion protection of 2024 aluminium alloy: a local electrochemical impedance approach, Corros. Sci. 101 (2015) 66–74, https://doi.org/10.1016/j.corsci.2015.09.002.

[10] H. Soliman, Influence of 8-hydroxyquinoline addition on the corrosion behavior of commercial Al and Al-HO411 alloys in NaOH aqueous media, Corros. Sci. 53 (2011) 2994–3006, https://doi.org/10.1016/j.corsci.2011.05.045.

[11] C. Verma, M. Quraishi, E. Ebenso, Quinoline and its derivatives as corrosion inhibitors: a review, Surf. Interfaces 21 (2020) 100634–100646, https://doi.org/10.1016/j.surfin.2020.100634.

[12] B. Fairman, A.S. Medel, Improved determination of aluminium species in waters using FIA separation/fluorimetric detection techniques, Int. J. Environ. Anal. 50 (1993) 161–171, https://doi.org/10.1080/03067319308027594.

[13] S.M. Li, H.R. Zhang, J.H. Liu, Corrosion behavior of aluminum alloy 2024-T3 by 8-hydroxy-quinoline and its derivative in 3.5% chloride solution, Trans. Nonferrous Met. Soc. 17 (2007) 318–325, https://doi.org/10.1016/S1003-6326(07)60092-2.

[14] I. Lukovits, E. Kalman, F. Zucchi, Corrosion inhibitors—correlation between electronic structure and efficiency, Corrosion 57 (2001) 3–8, https://doi.org/10.5006/1.3290328.

[15] G. Gece, Drugs: a review of promising novel corrosion inhibitors, Corros. Sci. 53 (2011) 3873–3898, https://doi.org/10.1016/j.corsci.2011.08.006.

[16] A. Kokalj, M. Lozinšek, B. Kapun, P. Taheri, S. Neupane, P. Losada-Pérez, C. Xie, S. Stavber, D. Crespo, F.U. Renner, A. Mol, I. Milošev, Simplistic correlations between molecular electronic properties and inhibition efficiencies: do they really exist? Corros. Sci. 179 (2021) 1–12, https://doi.org/10.1016/j.corsci.2020.108856.

[17] A. Kokalj, On the alleged importance of the molecular electron-donating ability and the HOMO–LUMO gap in corrosion inhibition studies, Corros. Sci. 180 (2021) 1–10, https://doi.org/10.1016/j.corsci.2020.109016.

[18] A. Kokalj, D. Costa, Molecular modeling of corrosion inhibitors, Ref. Modul. Chem. Mol. Sci. Chem. Eng. (2017), https://doi.org/10.1016/B978-0-12-409547-2.13444-4.

[19] A. Kokalj, On the estimation of standard adsorption free energy from corrosion inhibition efficiencies, 111139, Corros. Sci. 217 (2023) 1–7, https://doi.org/10.1016/j.corsci.2023.111139.

[20] Z. Fu, X. Guo, X. Zhang, D. Legut, D. Zhang, Towards rational design of organic copper corrosion inhibitors: high-throughput computational evaluation of standard adsorption Gibbs energy, Corros. Sci. 227 (2024) 111783, https://doi.org/10.1016/j.corsci.2023.111783.

[21] N. Kovacevic, I. Milosev, A. Kokalj, The roles of mercapto, benzene and methyl groups in the corrosion inhibition of imidazoles on copper: II. Inhibitor-copper bonding, Corros. Sci. 98 (2015) 457–470, https://doi.org/10.1016/j.corsci.2015.05.041.

[22] F. Chiter, C. Lacaze-Dufaure, H. Tang, N. Pébère, DFT studies of the bonding mechanism of 8-hydroxyquinoline and derivatives on the (111) aluminum surface, Phys. Chem. Chem. Phys. 17 (2015) 22243–22258, https://doi.org/10.1039/C5CP03095A.

[23] F. Chiter, M.-L. Bonnet, C. Lacaze-Dufaure, H. Tang, N. Pébère, Corrosion protection of Al (111) by 8-hydroxyquinoline: a comprehensive DFT study, Phys. Chem. Chem. Phys. 20 (2018) 21474–21486, https://doi.org/10.1039/c8cp03312a.

[24] Y. Bulteau, N. Tarrat, N. Pébère, C. Lacaze-Dufaure, 8-Hydroxyquinoline complexes (Alq3) on Al (111): atomic scale structure, energetics and charge distribution, N. J. Chem. 44 (2020) 15209–15222, https://doi.org/10.1039/D0NJ02824J.

[25] Y. Bulteau, C. Lepetit, C. Lacaze-Dufaure, Topological analysis of hydroxyquinoline derivatives interacting with aluminum cations or with an Al (111) surface, Inorg. Chem. 59 (2020) 17916–17928, https://doi.org/10.1021/acs.inorgchem.0c01972.

[26] F. Chiter, D. Costa, N. Pébère, P. Marcus, C. Lacaze-Dufaure, Insight at the atomic scale of corrosion inhibition: DFT study of 8-hydroxyquinoline on oxidized aluminum surfaces, Phys. Chem. Chem. Phys. 25 (2023) 4284–4296, https://doi.org/10.1039/d2cp04626a.

[27] G. Boisier, N. Portail, N. Pébère, Corrosion inhibition of 2024 aluminium alloy by sodium decanoate, Electrochim. Acta 55 (2010) 6182–6189, https://doi.org/10.1016/j.electacta.2009.10.080.

[28] J. Baux, N. Caussé, J. Esvan, S. Delaunay, J. Tireau, M. Roy, D. You, N. Pébère, Impedance analysis of film-forming amines for the corrosion protection of a carbon steel, Electrochim. Acta 283 (2018) 699–707, https://doi.org/10.1016/j.electacta.2018.06.189.

[29] D. Jero, N. Caussé, O. Marsan, T. Buffeteau, F. Chaussec, A. Buvignier, M. Roy, N. Pébère, Film-forming amines adsorption and corrosion kinetics on carbon steel surface in neutral solution investigated by EIS and PM-IRRAS analysis, Electrochim. Acta 443 (2023) 141925, https://doi.org/10.1016/j.electacta.2023.141925.

[30] M. Benoit, C. Bataillon, B. Gwinner, F. Miserque, M.E. Orazem, C.M. Sánchez-sánchez, B. Tribollet, V. Vivier, Comparison of different methods for measuring the passive film thickness on metals, Electrochim. Acta 201 (2016) 340–347, https://doi.org/10.1016/j.electacta.2015.12.173.

[31] S. Leleu, B. Rives, J. Bour, N. Causse, N. Pébère, On the stability of the oxides film formed on a magnesium alloy containing rare-earth elements, Electrochim. Acta 290 (2018) 586–594, https://doi.org/10.1016/j.electacta.2018.08.093.

[32] Gaussian 09, M.J. Frisch, G.W. Trucks, H.B. Schlegel, G.E. Scuseria, M.A. Robb, J.R. Cheeseman, G. Scalmani, V. Barone, B. Mennucci, G.A. Petersson, H. Nakatsuji, M. Caricato, X. Li, H.P. Hratchian, A.F. Izmaylov, J. Bloino, G. Zheng, J.L. Sonnenberg, M. Hada, M. Ehara, K. Toyota, R. Fukuda, J. Hasegawa, M. Ishida, T. Nakajima, Y. Honda, O. Kitao, H. Nakai, T. Vreven, J.A. Montgomery, Jr, J.E. Peralta, F. Ogliaro, M. Bearpark, J.J. Heyd, E. Brothers, K.N. Kudin, V.N. Staroverov, R. Kobayashi, J. Normand, K. Raghavachari, A. Rendell, J.C. Burant, S.S. Iyengar, J. Tomasi, M. Cossi, N. Rega, J.M. Millam, M. Klene, J.E. Knox, J.B. Cross, V. Bakken, C. Adamo, J. Jaramillo, R. Gomperts, R.E. Stratmann, O. Yazyev, A.J. Austin, R. Cammi, C. Pomelli, J.W. Ochterski, R.L. Martin, K. Morokuma, V.G. Zakrzewski, G.A. Voth, P. Salvador, J.J. Dannenberg, S. Dapprich, A.D. Daniels, Ö. Farkas, J.B. Foresman, J. V. Ortiz, J. Cioslowski, and D.J. Fox, Gaussian, Inc., Wallingford CT, 2009.

[33] G. Kresse, J. Hafner, Ab initio molecular dynamics for liquid metals, Phys. Rev. B 47 (1993) 558–561, https://doi.org/10.1103/PhysRevB.47.558.

[34] G. Kresse, J. Hafner, Ab initio molecular-dynamics simulation of the liquid-metal–amorphous-semiconductor transition in germanium, Phys. Rev. B 49 (1994) 14251–14269, https://doi.org/10.1103/PhysRevB.49.14251.

[35] G. Kresse, J. Furthmüller, Efficiency of ab-initio total energy calculations for metals and semiconductors using a plane-wave basis set, Comput. Mat. Sci. 6 (1996) 15–50, https://doi.org/10.1016/0927-0256(96)00008-0.

[36] G. Kresse, J. Furthmüller, Efficient iterative schemes for ab initio total-energy calculations using a plane-wave basis set, Phys. Rev. B 54 (1996) 11169–11186, https://doi.org/10.1103/PhysRevB.54.11169.

[37] J.P. Perdew, K. Burke, M. Ernzerhof, Generalized gradient approximation made simple, Phys. Rev. Lett. 77 (1996) 3865–3868, https://doi.org/10.1103/PhysRevLett.77.3865.

[38] F. Weigend, R. Ahlrichs, Balanced basis sets of split valence, triple zeta valence and quadruple zeta valence quality for H to Rn: design and assessment of accuracy, Phys. Chem. Chem. Phys. 7 (2005) 3297–3305, https://doi.org/10.1039/B508541A.

[39] F. Weigend, Accurate Coulomb-fitting basis sets for H to Rn, Phys. Chem. Chem. Phys. 8 (2006) 1057–1065, https://doi.org/10.1039/B515623H.

[40] S. Grimme, Semi empirical GGA-type density functional constructed with a long-range dispersion correction, J. Comput. Chem. 27 (2006) 1787–1799, https://doi.org/10.1002/jcc.20495.

[41] S. Grimme, J. Antony, S. Ehrlich, H. Krieg, A consistent and accurate ab initio parametrization of density functional dispersion correction (DFT-D) for the 94 elements H-Pu, J. Chem. Phys. 132 (2010) 154104–154111, https://doi.org/10.1063/1.3382344.

[42] A.V. Marenich, C.J. Cramer, D.G. Truhlar, Universal solvation model based on solute electron density and a continuum model of the solvent defined by the bulk dielectric constant and atomic surface tensions, J. Phys. Chem. B 113 (2009) 6378, https://doi.org/10.1021/jp810292n.

[43] C.P. Kelly, C.J. Cramer, D.G. Truhlar, SM6: a density functional theory continuum solvation model for calculating aqueous solvation free energies of neutrals, ions, and solute-water clusters, J. Chem. Theory Comput. 1 (2005) 1133–1152, https://doi.org/10.1021/ct050164b.

[44] A.V. Marenich, R.M. Olson, C.P. Kelly, C.J. Cramer, D.G. Truhlar, Self-consistent reaction field model for aqueous and nonaqueous solutions based on accurate polarized partial charges, J. Chem. Theory Comput. 3 (2007) 2011–2033, https://doi.org/10.1021/ct7001418.

[45] A.V. Marenich, C.J. Cramer, D.G. Truhlar, Universal solvation model based on solute electron density and on a continuum model of the solvent defined by the bulk dielectric constant and atomic surface tensions, J. Phys. Chem. B 113 (2009) 6378–6396, https://doi.org/10.1021/jp810292n.

[46] J.D. Thompson, C.J. Cramer, D.G. Truhlar, Predicting aqueous solubilities from aqueous free energies of solvation and experimental or calculated vapor pressures of pure substances, J. Chem. Phys. 119 (2003) 1661–1670, https://doi.org/10.1063/1.1579474.

[47] J.P. Perdew, K. Burke, M. Ernzerhof, Generalized gradient approximation made simple, 1396, Phys. Rev. Lett. 78 (1997) 1396, https://doi.org/10.1103/PhysRevLett.78.1396.

[48] P.E. Blöchl, Projector augmented-wave method, Phys. Rev. B 50 (1994) 17953–17979, https://doi.org/10.1103/PhysRevB.50.17953.
[49] G. Kresse, D. Joubert, From ultrasoft pseudopotentials to the projector augmented-wave method, Phys. Rev. B 59 (1999) 1758–1775, https://doi.org/10.1103/PhysRevB.59.1758.
[50] M. Methfessel, A. Paxton, T, High-precision sampling for Brillouin-zone integration in metals, Phys. Rev. B 40 (1989) 3616–3621, https://doi.org/10.1103/PhysRevB.40.3616.
[51] H.J. Monkhorst, J.D. Pack, Special points for Brillouin-zone integrations, Phys. Rev. B 13 (1976) 5188–5192, https://doi.org/10.1103/PhysRevB.13.5188.
[52] S. Peljhan, J. Koller, A. Kokalj, The effect of surface geometry of copper on adsorption of benzotriazole and Cl. Part I, J. Phys. Chem. C. 118 (2014) 933–943, https://dx.doi.org//10.1021/jp409717e.
[53] M. Poberžnik, D. Costa, A. Hemeryck, A. Kokalj, Insight into the bonding of silanols to oxidized aluminum surfaces, J. Phys. Chem. C. 122 (2018) 9417–9431, https://doi.org/10.1021/acs.jpcc.7b12552.
[54] N. Kovačević, A. Kokalj, The relation between adsorption bonding and corrosion inhibition of azole molecules on copper, Corros. Sci. 73 (2013) 7–17, https://doi.org/10.1016/j.corsci.2013.03.016.
[55] K. Mathew, R. Sundararaman, K. Letchworth-Weaver, T.A. Arias, R.G. Hennig, Implicit solvation model for density-functional study of nanocrystal surfaces and reaction pathways, J. Chem. Phys. 140 (2014) 084106, https://doi.org/10.1063/1.4865107.
[56] K. Mathew, V.S.C. Kolluru, S. Mula, S.N. Steinmann, R.G. Hennig, Implicit self-consistent electrolyte model in plane-wave density-functional theory, J. Chem. Phys. 151 (2019) 234101, https://doi.org/10.1063/1.5132354.
[57] W. Tang, E. Sanville, G. Henkelman, A grid-based Bader analysis algorithm without lattice bias, J. Phys.: Condens. Matter 21 (2009) 084204, https://doi.org/10.1088/0953-8984/21/8/084204.
[58] K. Momma, F. Izumi, VESTA: a three-dimensional visualization system for electronic and structural analysis, J. Appl. Crystallogr. 41 (2008) 653–658, https://doi.org/10.1107/S0021889808012016.
[59] K. Momma, F. Izumi, VESTA 3 for three-dimensional visualization of crystal, volumetric and morphology data, J. Appl. Crystallogr. 44 (2011) 1272–1276, https://doi.org/10.1107/S0021889811038970.
[60] A. Kokalj, S. Peljhan, M. Finšgar, I. Milošev, What determines the inhibition effectiveness of ATA, BTAH, and BTAOH corrosion inhibitors on copper? J. Am. Chem. Soc. 132 (2010) 16657–16668, https://doi.org/10.1021/ja107704y.
[61] S. Trasatti, L.M. Doubova, Crystal-face specificity of electrical double-layer parameters at metal/solution interfaces, J. Chem. Soc Faraday Trans. 91 (1995) 3311–3325, https://doi.org/10.1039/FT9959103311.
[62] E. Bardez, I. Devol, B. Larrey, B. Valeur, Excited-state processes in 8-hydroxyquinoline: photoinduced tautomerization and solvation effects, J. Phys. Chem. B 101 (1997) 7786–7793, https://doi.org/10.1021/jp971293u.
[63] J. Fresco, H. Freiser, Stabilities of chelates of certain substituted 8-quinolinols, Inorg. Chem. 2 (1963) 82–85, https://doi.org/10.1021/ic50005a023.
[64] T. Le Bahers, C. Adamo, I. Ciofini, Theoretical determination of the pKas of the 8-hydroxyquinoline-5-sulfonic acid: a DFT based approach, Chem. Phys. Lett. 472 (2009) 30–34, https://doi.org/10.1016/j.cplett.2009.02.072.
[65] N. Tarrat, M. Benoit, M. Giraud, A. Ponchet, M.J. Casanove, The gold/ampicillin interface at the atomic scale, Nanoscale 7 (2015) 14515–14524, https://doi.org/10.1039/C5NR03318G.
[66] X. Fenouillet, M. Benoit, N. Tarrat, On the role of intermolecular interactions in stabilizing AuNP@Ampicillin nano-antibiotics, Materialia 4 (2018) 297–309, https://doi.org/10.1016/j.mtla.2018.09.036.
[67] M. Muccini, M.A.L.K. Kenevey, R. Zamboni, N. Masciocchi, A. Sironi, Blue luminescence of facial Tris(quinolin-8-olato)aluminum(III) in solution, crystals, and thin films, Adv. Mater. 16 (2004) 861–864, https://doi.org/10.1002/adma.200305421.
[68] A.K. Saxena, Solid State Preparation of the (8-Hydroxyquinolinato)Aluminum(Iii) Complex from Aluminum Isopropoxide and 8-Hydroxyquinoline, Synth. React. Inorg. Met. Org. Chem. 29 (1999) 1747–1767, https://doi.org/10.1080/00945719909351733.
[69] G. Gece, The use of quantum chemical methods in corrosion inhibitor studies, Corros. Sci. 50 (2008) 2981–2992, https://doi.org/10.1016/j.corsci.2008.08.043.
[70] T.E. Daubert, R.P. Danner, Physical and Thermodynamic Properties of Pure Chemicals: Data Compilation, Taylor & Francis, Washington, DC et, 1989.
[71] M.A.V. Ribeiro da Silva, M.J.S. Monte, M.A.R. Matos, Enthalpies of combustion, vapour pressures, and enthalpies of sublimation of 8-hydroxyquinoline, 5-nitro-8-hydroxyquinoline, and 2-methyl-8-hydroxyquinoline, J. Chem. Thermodyn. 21 (1989) 159–166, https://doi.org/10.1016/0021-9614(89)90127-4.
[72] M.A.V. Ribeiro da Silva, M.J.S. Monte, Vapour pressures and enthalpies of sublimation of six halogen-substituted 8-hydroxyquinolines, J. Chem. Thermodyn. 24 (1992) 715–724, https://doi.org/10.1016/S0021-9614(05)80078-3.
[73] https://pubchem.ncbi.nlm.nih.gov.
[74] A. Kokalj, Molecular modeling of organic corrosion inhibitors: why bare metal cations are not appropriate models of oxidized metal surfaces and solvated metal cations, Acta Chim. Slov. 61 (2014) 340–349. ⟨https://acta-arhiv.chem-soc.si/61/61-2-340.pdf⟩.